Preprint
UCRL-JC-152890

Electron Cyclotron Heating and Current Drive for Maintaining Minimum q in Negative Central Shear Discharges

T.A. Casper, T.B. Kaiser, R.A. Jong, L.L. LoDestro, J. Moller, L.D. Pearstein

This article was submitted to: Plasma Physics and Controlled Fusion

U.S. Department of Energy

Lawrence
Livermore
National
Laboratory

April 2003

Approved for public release; further dissemination unlimited

DISCLAIMER

This document was prepared as an account of work sponsored by an agency of the United States Government. Neither the United States Government nor the University of California nor any of their employees, makes any warranty, express or implied, or assumes any legal liability or responsibility for the accuracy, completeness, or usefulness of any information, apparatus, product, or process disclosed, or represents that its use would not infringe privately owned rights. Reference herein to any specific commercial product, process, or service by trade name, trademark, manufacturer, or otherwise, does not necessarily constitute or imply its endorsement, recommendation, or favoring by the United States Government or the University of California. The views and opinions of authors expressed herein do not necessarily state or reflect those of the United States Government or the University of California, and shall not be used for advertising or product endorsement purposes.

This is a preprint of a paper intended for publication in a journal or proceedings. Since changes may be made before publication, this preprint is made available with the understanding that it will not be cited or reproduced without the permission of the author.

Electron Cyclotron Heating and Current Drive for Maintaining Minimum q in Negative Central Shear Discharges

T.A. Casper, T.B. Kaiser, R.A. Jong, L.L. LoDestro, J. Moller, and L.D. Pearlstein
Lawrence Livermore National Laboratory, Livermore, California, USA
Dodge, T. *University of California-Davis*

Abstract

Toroidal plasmas created with negative magnetic shear in the core region offer advantages in terms of MHD stability properties. These plasmas, transiently created in several tokamaks, have exhibited high performance as measured by normalized stored energy and neutron production rates. A critical issue with extending the duration of these plasmas is the need to maintain the off-axis-peaked current distribution required to support the minimum in the safety factor q at large radii. We present equilibrium and transport simulations that explore the use of electron cyclotron heating and current drive to maintain this negative shear configuration. Using parameters consistent with DIII-D tokamak operation [1,2], we find that with sufficiently high injected power, it is possible to achieve steady-state conditions employing well aligned electron cyclotron and bootstrap current drive in fully non-inductively current-driven configurations.

I. Introduction

High-performance, fusion-relevant discharges are created in several tokamaks [1-5] with various optimized magnetic shear configurations exhibiting internal transport barriers (ITB) resulting from a reduction in transport due to the decreasing magnetic shear in the interior of the core region. Negative central shear (NCS) discharges are transiently created in DIII-D [1,2] during the Ohmic current ramp-up by auxiliary heating and current drive from neutral-beam injection. Both q_{min}, the minimum of the dimensionless safety factor q, and the radial location at which it occurs, ρ_{qmin} [ρ= sqrt(normalized toroidal flux) ~ r/a, a=minor radius], decrease with time as the Ohmically induced flux diffuses inward, peaking the current near the magnetic axis. A critical issue for sustaining high-performance NCS discharges is the ability to maintain the total current density profile, J_T, with an off-axis maximum. Sustaining such hollow current profiles in steady state requires use of non-inductive current-drive sources such as neutral beams (NBCD), radio frequency (RF), or bootstrap (BSCD) current. The electron cyclotron heating (ECH) and current drive (ECCD) system on DIII-D, recently upgraded to six gyrotron sources [6], provides more than 4MW of power for long-pulse operation useful for sustaining this required off-axis-peaked current distribution. This upgrade supports a long-range goal to use ECH and/or ECCD to sustain high-performance discharges with high values of normalized β, confinement enhancement factor H, and neutron production rates with bootstrap current fractions, $f_{bs}=I_{BS}/I_T$, in excess of 50% where $\beta=nkT/(B^2/2\mu_0)$, $\beta_N=\beta/(I_p/aB_T)$, T=thermal temperature, B=magnetic field, and n=particle density. While NCS has provided enhanced stability to many kinetic modes, these high-performance, ITB discharges often exhibit significant peaking of the pressure profile. This pressure peaking can drive MHD modes that spoil confinement and thus require control of plasma profiles if we are to extend this operation to long pulse or to steady state. To demonstrate the feasibility of ECH/ECCD for current profile control in these ITB discharges and to investigate what is possible with the DIII-D EC system, we use time-dependent simulations of the equilibrium, transport and stability. We are exploring methods to alter q through direct current drive along with localized electron heating to modify the bootstrap current drive profile.

In simulations presented here, we explore parametric dependencies of the heating, current drive, and profiles that affect our ability to maintain the desired q-profile in these NCS discharges. We primarily use the Corsica equilibrium and transport code [7-10]. In Corsica, we self-consistently and simultaneously converge equilibrium and transport during the temporal evolution using source models for neutral-beam and electron-cyclotron heating and current drive that are also evaluated at each time step. The equilibrium is provided by a solution to the Grad-Shafranov equation using the evolved pressure profile obtained from a combination of measured and transported fields. We use Corsica to predict the temporal evolution of the current density from an initial measured experimental state using a combination of sources, thermal transport models and neoclassical resistivity. We use experimental measurements of the electron density, n_e, and the effective charge state, Z_{eff}, assuming a fully ionized carbon impurity and determine the thermal-particle density profiles from quasi-neutrality including the fast ions from neutral-beam injection (NBI). We model the neutral-beam injection using the NFREYA [11] code that determines the heating power, current drive and fast-ion density from a Monte Carlo calculation. This deposition model uses detailed beam-particle orbit calculations to determine contributions from the particle residence time on each flux surface. A slowing-down distribution for the fast ions is assumed. In these simulations we use no fast-ion diffusion. Fast-ion diffusion is often used in Corsica and other codes to simulate the effects of Alfven and/or MHD instabilities on the beam-ion distribution. We calculate the bootstrap current drive using a neoclassical model obtained from the NCLASS code [12]. For the ECH/ECCD physics, we use either an analytic model or a ray-tracing calculation from the TORAY-GA code [13-15]. Using these predictive capabilities, we explore methods for increasing the duration, τ_{dur}, and radius, ρ_{qmin}, that the NCS configuration can be sustained by control of the local current-density profile via simulations of the electron-cyclotron heating and current drive for DIII–D-like parameters.

To evolve entropy profiles (electron, T_e, and ion, T_i, temperature profiles), we use a thermal diffusivity model based on the gyro-Bohm scaling [16] to provide the parametric dependence of confinement on the plasma conditions. In our model, the electron heat diffusivity is given by $\chi_e=c_e(T_e^{3/2}/B^2)(T_e/T_i)^{\alpha}f(s)q^2+\chi_e^{neo}+\chi_{edge}$ where $s=(\rho/q)\partial q/\partial\rho$ is the shear parameter and $f(s)=1/[1+(9/4)(s-2/3)^2]$ is used to simulate shear dependence representative of results from gyro-fluid simulations [17]. We choose $c_e=1.4$ to approximate the experimentally measured electron temperature profile in the absence of EC power and $\alpha=1$ is used for the temperature- ratio dependence in these simulations. We obtain the electron neoclassical diffusivity, χ_e^{neo}, from the NCLASS model. χ_{edge} provides control of the edge heat diffusivity consistent with edge modeling and convergence requirements. This representation provides a weak electron thermal transport barrier. The ion thermal diffusivity model is, $\chi_i = c_i\chi_e H(\nabla q)Z_{eff}(T_e/T_i)^{1/2}+\chi_i^{neo}$ where c_i=1.0, χ_i^{neo} is the ion neoclassical heat diffusivity from NCLASS and $H(\nabla q)$ is the Heaviside function which turns on at ρ_{qmin}. This model gives a strong ion thermal transport barrier at $\rho_{q\mathrm{min}}$, qualitatively consistent with experimental observations [2-5,18], theory [19] and global fluid simulations [20]. Inside the barrier, this model has ion transport that is neoclassical while outside the barrier it allows independent scaling of χ_i to better approximate the measured ion temperature profiles. While this model was stimulated by transport measurements on several experiments, our intention is not to do a detailed investigation of transport models or fitting to data but rather to provide a credible model for heat diffusivity that reasonably well approximates measured profiles while allowing for simulation of the effects of electron-cyclotron heating and current drive on barriers in NCS configurations. We adjust free parameters (c_e, c_i) in the model to obtain a reasonable representation of the electron and ion temperature profiles consistent with those measured in selected DIII–D shots. These constants were held fixed for all simulations. Fluctuation-based transport models such as GLF23 [21] are just beginning to show promise at predicting the occurrence and properties of internal transport barriers.

Although different discharges have been simulated, we concentrate here on the DIII–D shot 92668 conditions since it is representative of an experimental series of high performance NCS discharges with L-mode edges [2, 18]. Typically, these shots rise to high neutron reactivity but eventually disrupt without additional control due to very peaked pressure profiles. In Figure 1, we show plasma parameters for this shot and indicate the time at which we initialize simulation profiles and plasma shape. We initialize these simulations at 1.45s where high performance conditions were experimentally achieved. We use the measured density, temperature, and Z_{eff} profiles and the boundary shape as determined from an EFIT [22] equilibrium calculated using both magnetic and motional Stark effect measurement constraints. By converging the free boundary equilibrium solution in Corsica to the EFIT solution we achieve essentially exact agreement between Corsica and EFIT for the plasma shape and initial q-profile. In Figure 2(a) we show a comparison of the experimental q-profile (EFIT/MSE) and the Corsica equilibrium at 1.46s using the transported temperature profiles shown in Figure 2(b). The ion and electron thermal conductivities obtained from our model are shown in Figure 2(c). We also show in Figure 2(b) a comparison of the measured temperature profiles with those obtained from our transport model (no ECH or ECCD). These time-evolved temperature profiles indicate that the transport model provides a reasonably good model for the thermal transport without ECH. The small difference in the q profiles in Figure 2(a) comes from the use of transported temperature profiles, Figure 2(b), in Corsica to calculate this q profile. From this initial state, we use a fixed boundary equilibrium calculation including resistive current evolution (Ohm's law) to evolve the current density and q profiles along with the temperature profile changes resulting from the intense heating. We can time-dependently assess the ideal MHD stability of the resulting equilibria with the DCON [23] stability code that has been added to the Corsica suite.

II. Parametric study using an analytic model for EC deposition.

In order to more rapidly explore sensitivity to parametric variations of the heating and current drive, we ran a series of simulations using a Gaussian approximation for the ECH power deposition and current drive profiles. For these analytic modeling studies, we use the standard scaling relationship for RF current drive, $I_{ECCD}=\gamma P_{EC} T_e/n_e R$, to determine the ECCD, where the efficiency, γ, and Gaussian shape parameters are estimated from experiments [24]. P_{EC} is the absorbed power (total integrated Gaussian power density) and we use a width of $\delta\rho=0.05$ ($\delta r\sim 3$ cm) in minor radius. After demonstrating the desired current drive effects with this simpler analytic modeling, selected simulations are repeated (Section III) with the EC ray tracing code, TORAY-GA, to incorporate the ray propagation (launch geometry and refraction) and linear absorption physics into a more realistic simulation of the heating and current drive. This introduces additional complications due to movement of the deposition and current drive layer resulting from EC modification of the electron temperature profile and the equilibrium via the driven current distribution. As we will show, ray tracing requires the use of feedback control on the EC launch to maintain the desired current-drive profile and, therefore, its effects. The experimental capability for this real-time control is being added to some of the existing antennas on DIII-D.

We performed several simulations for the DIII-D shot 92668 conditions shown in Figure 1. The DIII-D tokamak has a major radius of 1.78m with a minor radius a=0.64m. For this 1.4MA shot, we operated at a toroidal field of B_T=2.1T in a shaped, upper-single-null configuration with elongation ε=1.71 and upper triangularity δ_U=0.78. We injected 10MW of neutral-beam power driving current along the Ohmic current (co-NBI) resulting in on-axis temperatures of 6keV for electrons and 19keV for ions and a peak electron density of $0.7\text{x}10^{20}\text{m}^{-3}$. These parameters are representative of several high-performance negative central shear discharges having L-mode edge density profiles. Simulations are initialized at 1.45s into the discharge, just prior to a β-collapse resulting from MHD activity due to the internally peaked pressure profile resulting from density profile peaking obtained with neutral-beam fueling and heating. The β-collapse can be avoided experimentally by feedback control of the neutral-beam power to limit the plasma pressure or possibly by density changes often observed when EC power is injected inside a transport barrier [25,26]. Using the analytic model, we varied the EC heating power and location to investigate effects on the NCS configuration, in particular, on the duration, τ_{dur}, that the q profile can be maintained by modification of the current profile. Through a combination of direct ECCD and electron heating to increase the temperature gradient and thus the bootstrap current, we find that this NCS configuration can be maintained for durations much longer than several energy confinement times and longer than the current relaxation time, provided sufficient power is absorbed. The local peaking of the current density profile (and therefore a depression in q) maintains the location of ρ_{qmin} and thus sustains the barrier [16]. In these simulations we turn on EC power at 1.5 seconds and force the boundary (separatrix) loop-voltage to zero in order to turn off the transformer (Ohmic) drive to find fully non-inductively-driven steady-state conditions. We simulated EC absorbed power levels between 0 and 15MW with the neutral-beam power held fixed at P_{NB}=10MW. The 2.3MW case (3MW injected) corresponds to power levels routinely available on DIII-D (4MW injected has been achieved) and the 4.5MW (6MW injected) a future upgrade.

In Figure 3, we show the radial profiles at a few selected times of the total flux-averaged current density, $<J_T>=<J•B>/<B•\nabla\psi>$, and the resulting q profiles achieved for the 4.5MW case with power applied at ρ=0.425, just inside the ρ_{qmin} formed with early neutral-beam injection during the current ramp on DIII-D. When ECH is applied at 1.5s, initially there is no perturbation in the total current profile due to inductive cancellation of the driven current. By 1.6s, there is a noticeable peaking of the total current from the non-inductively driven EC current that results in a local depression in the q profile along with inductively induced changes near the magnetic axis. This modification in the q profile persists as the ECCD is maintained. As the flux diffuses inward, the Ohmic current density (J_{OH}) becomes more peaked towards the magnetic axis and effectively cancels out a portion of the NBCD; this allows q_0 to rise with time. As this Ohmic current resistively dissipates over time (Ohmic drive is turned off in these simulations by forcing the loop voltage to be zero at the separatrix), the NBCD begins to dominate the total current density distribution near the axis and q_0 begins to fall. The rise in J_T between the magnetic axis and the ECCD peak at ρ=0.425 is a result of the bootstrap current drive. Depending on the location and magnitude of the bootstrap current peak, that is, the bootstrap current alignment with respect to width of the on-axis-peaked NBCD and the location of the ECCD, q_{min} can be maintained for some length of time, τ_{dur}. If the alignment and magnitude of the current drive components are not properly adjusted, the q_{min}, and therefore the barrier location, will move inward and ultimately be lost as J_{OH} decays. In Figure 4, we show the current density profile components from the various sources at t=4.0s, just prior to losing the ability to maintain the barrier at the power level simulated. At this time, a volume-averaged total current of I_p=1.43MA is produced by the EC-current drive of I_{EC}=0.19MA plus a bootstrap current of I_{BS}=0.59MA, neutral-beam-driven current of I_{NB}=0.83MA and a residual Ohmic current of I_{OH}=-0.18MA. Since we are not controlling the plasma current (0 edge loop voltage control), the plasma current is free to change in time and is determined from the non-inductive current drive present with the Ohmic current resistively dissipating. We note that the Ohmic current has decayed to essentially zero in the more resistive outer half of the plasma but remains large in the hot interior region (and negative due to the over drive by the neutral beam current). At the 4.5MW power level for the heating location at ρ=0.425, the NCS configuration is maintained for a duration τ_{dur}~3.2s (to t~4.7s). At late times, the Ohmic current decays to zero over the entire cross-section and the total internal current distribution is determined by a combination of the bootstrap, electron-cyclotron and neutral-beam non-inductively-driven currents. The NBCD profile is peaked on axis for the injection geometry on DIII-D. If present, fast-ion diffusion would broaden the on-axis NBCD profile and reduce its magnitude. Details of the current profile evolution near the axis would be different but still dominated by the NBCD since the bootstrap current is small in the vicinity of the magnetic axis and the ECCD is being driven off-axis. The overall effect on the q-profile evolution near the heating location and q_{min} would not be affected. We choose to simulate conditions without fast ion spreading to explore evolution in the absence of instabilities believed to be the source of the fast ion diffusion.

As a figure of merit of the capability for ECCD to hold the barrier, we use the time duration τ_{dur} that ρ_{qmin} is held fixed just outside the EC deposition location. Due to the on-axis peaking and dissipation of the Ohmic current, at low to moderate EC power levels the position of q_{min} eventually moves in at the current evolution rate [16] as indicated in Figure 5, where we show the evolution of q_{min} and ρ_{qmin} for various EC powers applied. The evolution of q_{min} is determined by the relative contributions due to ECCD, BSCD and NBCD near the heating location. The sharp break in the ρ_{qmin} vs. time curve is the transition from a local minimum supported by ECCD to that maintained by the internal current distribution formed by the combined effect of the non-inductive current drive components; for example, see the q profile at 4s and 7s shown in Figure 3. We summarize in Figure 6 a series of simulations using the analytic EC model where the power and heating location is varied. We observe that when power is absorbed at the $\rho=0.425$ location, good alignment of the ECCD with the bootstrap current allows us to create the desired off-axis peaked current profile and thus maintain ρ_{qmin} for much longer duration than when heating at $\rho=0.5$, the location just outside the initially formed barrier. Ultimately, the NCS configuration is either lost due to on-axis peaking of the current density resulting from the NBCD or the q profile drops below 1 at some radius at which time the simulations are stopped (since sawtooth activity would be expected to alter the current distribution). We observe that at P_{EC}~8MW at $\rho=0.425$ we can sustain the barrier for intervals of a few hundred energy-confinement times, τ_E~0.1s. For the DIII-D neutral-beam injection geometry, steady-state operation will, however, require additional on-axis current-profile control to counteract the NBCD and thus maintain higher values of q_0 and q_{min}.

To explore the effects of density control on performance, we ran simulations with the experimental density profile scaled to 90% and to 80% of the measured values for the case with ECCD at $\rho=0.425$. The additional power per particle available increases the current drive and provides a further enhancement of the efficacy of ECH for sustaining such NCS discharges. As observed in Figure 6 for 4.5MW, we obtain a factor of 5 increase in duration that the NCS configuration can be sustained at 80% density. To further explore the advantages of density profile control, we used a model density profile of the form $n(\rho)=n_0/(1+ a_\rho(\rho/\rho_0)^2)$ (rather than scaling the measured profile) with the peak density set to the measured value of $0.7\text{x}10^{20}$. This model profile was adjusted to place the density gradient near the heating location to optimize the location of the density-gradient-driven bootstrap current and provide better alignment of the overall desired total current profile. In Figure 6, we note a further increase in the duration that the NCS configuration can be maintained to ~7.5 times longer than when using the full measured density profile. This advantage is one motivation for exploring density control in experiments and for our beginning to do simulations with core transport coupled to the UEDGE [27] code.

Using the DCON stability code, we assessed ideal MHD stability during simulated discharge evolution. DCON is an energy-principle code that calculates the minimum potential energy, δW, to determine overall stability to ideal MHD internal and external modes; it also assesses ballooning-mode stability. In Figure 7, we show the time evolution of δW_{total} (= $\delta W_{plasma}+\delta W_{vacuum} > 0$ for stability) for toroidal mode numbers n=1,2 and 3 for the 4.5MW case with ECCD at $\rho=0.425$. We note that shortly after initialization at the time EC power is applied, 1.5s, DCON predicts instability for all three mode numbers and, indeed, the actual experimental discharge experienced a β-collapse at 1.57s due to peaking of the pressure profiles as we transiently maximized the neutron production rate in this shot. During the formation phase of the self-consistently driven current profile shortly after ECH is applied ($1.5<t<2.3$s), we observe these mode numbers are initially stabilized but then become unstable again at t~2s. This is likely due to the strongly locally perturbed q profile resulting from the formation of a highly peaked current density profile at the ECH location. As the q profile continues to evolve, stability is regained, $\delta W_{total} > 0$, for all three mode numbers at t~2.3s and maintained for the duration of the simulation until the barrier is lost at t~4.7s for these parameters. One effect of the ECH heating is to broaden the electron temperature profile out to the heating location at $\rho=0.425$. The combined effect of heating and the transport model is to provide a relatively flat temperature profile inside the location of minimum q. The broadened temperature profile and modification in the parallel current distribution due to ECCD have resulted in the MHD stability. We observe destabilization of the n=3 mode at the time the barrier was lost for both 3MW and 4.5MW simulations. A detailed study of barrier stability is beyond the scope of this paper. The prediction of instability during the early part of the evolution indicates the possible need for spreading the ECCD profile in actual q-profile control experiments. This can be achieved with multiple gyrotron sources by aiming the EC antennas at slightly different poloidal and/or toroidal angles as is currently possible on DIII-D.

Using this analytic ECH/ECCD model for a survey of parameters, we have identified the beneficial effect of electron cyclotron heating and current drive for maintaining the barrier for long durations in NCS discharges. These results serve to guide our selection of parameter space and demonstrate a desired result. With ECCD applied just inside the barrier location, $\rho=0.425$, we are able to maintain the barrier for several hundred energy confinement times. We will now focus on this deposition location and use TORAY-GA ray-tracing modeling of ECH/ECCD to explore additional physics issues associated with EC launch, propagation and linear absorption to get better estimates of the current drive profiles and efficiencies.

III. Propagation effects on barrier control with ECH/ECCD localized at $\rho=0.425$

In our survey of EC effects on these NCS discharges with L-mode edge conditions, we scanned the deposition location over the range $0.2 < \rho < 0.7$ [16]. Deposition near $\rho=0.425$ provided the best performance in terms of maintaining the barrier duration and radial extent. This performance results from a combination of good absorption efficiency for both heating and current drive for the electron density and temperature profiles at this location and from the alignment of ECCD with the decreasing bootstrap current density as shown in Figure 4. ECCD near the peak of the bootstrap current drive profile maintains the barrier for slightly longer durations but results in smaller barrier regions and, therefore, lower performance. For these reasons, we chose these conditions to study propagation effects, an issue critical to an experimental demonstration of the efficacy of ECCD. We use the TORAY-GA code [13-15] to model the propagation physics and linear absorption for the EC geometry [6] on the DIII-D experiment. Heating and current drive are determined from the linear absorption at the 2nd harmonic resonance for 110GHz, the gyrotron source frequency on DIII-D. The TORAY-GA code with its linear absorption model has been shown to give good agreement with experimental measurements for most DIII-D conditions [24]. Under some conditions, non-linear effects can reduce the current drive efficiency by ~10-15%.

This would have only minimal effect on the conclusions and simulation results shown here.

The ECH launch geometry is determined from the poloidal, θ_{EC}, and toroidal, ϕ_{EC}, launch angles from an antenna located at x_{EC}=2.39m and z_{EC}=0.71m for DIII-D as is indicated schematically in Figure 8. As we will show, feedback control of the poloidal launch angle is required to achieve the desired current-drive effects. This capability is currently being added to the antenna system used on DIII-D. The trajectory plots shown in Figure 8 are representative of the simulations presented here. The ray paths include the effects of refraction from the local density profiles for the equilibrium surfaces shown. The ray paths terminate when the power is reduced to 10^{-4} times the launched power and represents the location where the incident power is fully absorbed. We varied the antenna angles to obtain heating and current drive profiles centered at ρ=0.425 and similar in shape to those used for the analytic model in our previous survey of current drive effects.

IIIa Simulations without feedback of antenna aiming

We performed simulations to obtain current-drive profiles consistent with those of the analytic model at ρ=0.425 by scanning the antenna aiming angle using the density and temperature profiles at initialization (1.45s). Fixing the aiming at these angles, we then scanned the EC power absorbed as was done with the analytic model to determine effects on the barrier. For our gyro-Bohm thermal transport model, we observe a modification of the temperature profile by ECH and changes in the equilibrium by both the modified bootstrap current and the direct ECCD that result in time-dependent changes in the location of the resonant absorption of the EC power. Both the local cyclotron resonance and Doppler shifting of the resonance by the higher electron thermal velocity play a role in this change. The net result is that the location of the peak current drive tends to move outward with time, Figure 9a feedback off, to locations where the current drive efficiency is reduced both by less favorable local plasma conditions (lower T_e) and trapped particle effects [28,29]. The heating rate, however, is maintained and this, in turn, maintains the electron temperature and bootstrap current profiles but the direct ECCD is reduced. The overall effect is that even at very high EC powers, we are not able to sustain the barrier due to these modifications of the absorption conditions as we show in the "toray no feedback" performance curve in Figure 6.

IIIb Antenna feedback simulations

To regain performance, we implemented a feedback algorithm in the simulation to adjust the poloidal and toroidal antenna aiming angles to maintain the desired location of the current drive in the presence of these changing absorption conditions. While feedback in the simulation was developed to control both the toroidal and poloidal aiming, only control of the poloidal angle is required here. Capability for real-time control of the antennas is currently under development with testing expected to begin soon. Alternatively, feedback on the plasma position and/or the toroidal magnetic field could be used but these have not been implemented in the simulations. A predictor/corrector technique using the location of peak ECCD was used to modify the EC aiming at each time step in the simulation. While Corsica employs a variable time-stepping technique, for these simulations we limited the time step size to 10ms and corrected the antenna aiming at this rate. With this ability to feedback control the position of the ECCD, we are able to maintain ρ_{qmin} as in the analytic model case. We show this power scan for ECCD at ρ=0.425 as the "toray feedback" curve in Figure 6 and note that comparable performance with the ray tracing code requires additional EC power. This additional power comes from the modification of the current drive and heating profiles as the resonance conditions change in time due to the changing equilibrium. It is also due in part to experimental difficulties and uncertainties in determining the current drive efficiency and the effective Gaussian width used for the analytic model. We observe that at P_{EC}=12MW we can maintain the barrier to essentially steady state, a duration of 25s shown in Figure 6 and, as is indicated in Figure 10, by the evolution of ρ_{qmin} for the scan in injected power using Toray-GA.

We show in Figure 9a the effect of the feedback on the ECCD profile near the control location of ρ=0.425 and the corresponding q profiles in Figure 9b. As can be seen, the ECCD without feedback continues to move to larger radii where the current drive amplitude is reduced. There is a pronounced effect on the q_{min} just outside of the ECCD location and ρ_{qmin} moves outward slightly. Again, the q profile near the magnetic axis also changes due to inductive effects and these are significantly different with and without feedback due to differences in the resulting direct current drive. From Figures 6 and 10 we conclude that the optimum power in these simulations for maintaining the barrier is about 12MW where ρ_{qmin} can be sustained essentially indefinitely. At higher power levels, e.g. the 15MW case, the ECCD is sufficient to drive q_{min} less than 1 whereas at lower powers, e.g. the 11.25MW case, the inward movement and dissipation of the peak Ohmic current ultimately causes the barrier to be lost (q_{min} moves inward and the barrier location is locked to q_{min} for this transport model). In the 12MW feedback simulation, the total angular excursion of the antenna during control was 10 degrees poloidally. With the antenna aiming above the midplane, Figure 8a, it’s motion to larger poloidal angles tends to force the EC-driven current to smaller ρ to compensate for the broadening temperature profiles. While the simulation allowed for angular aiming adjustments at a 10ms rate, after an initial transient, the actual corrections were made at the much slower rate of 1 to 4 seconds. A similar study using lower hybrid waves in place of EC current drive was done by Dumont et al. [30]. In Figure 11, we show the current profiles at 20s for the 12MW case where the alignment of the ECCD and bootstrap currents is evident. At this time, the q profile achieves an overall minimum that is just slightly greater than one. The 1.57MA plasma current is essentially all non-inductively driven with I_{EC}=0.46MA due to direct EC current drive, I_{BS}=0.6MA sustained by the temperature and density gradients resulting from transport combined with neutral beam and EC heating, and I_{NB}=0.58MA coming from the tangentially aimed neutral beams. There still remains –0.07MA of residual Ohmic current that is slowly dissipating in time. This configuration can be maintained to steady state. We note that in all cases while the barrier is being sustained, there is good alignment between the ECCD and BSCD which creates an off-axis-peaked current-drive profile as is needed to sustain ρ_{qmin} at the barrier. Thus, with the addition of feedback control on the antenna aiming, we are able to maintain the barrier as was obtained with the analytic simulations. In these simulations, we are altering the NCS current density profile obtained by early NBI during the Ohmic current ramp and this leads to moderately high EC power levels. We have not attempted to optimize the current profile during startup which may lead to lower power requirements for these NCS plasmas. Simulations based on other high-performance discharges [31] also indicate that it may be possible to sustain the current profile at lower EC power levels.

IV. Summary

These time-dependent simulations of electron-cyclotron heating and current drive indicate that, by absorbing sufficiently high power at the electron cyclotron-frequency, the internal transport barriers associated with L-mode-edge NCS discharges can be sustained for very long durations, several hundred τ_E or to steady state, by controlling the current profile. Configurations exhibit a fully non-inductively-driven state formed from a well-aligned combination of bootstrap, neutral-beam and electron-cyclotron current drive. Ideal MHD stability calculations indicate a stable configuration can be achieved at steady state, but additional control may be needed to maintain stability over the full duration evolution. Primarily due to the peaked density profile associated with L-mode edge conditions plus moderate electron temperatures at ρ~0.4, ECCD plays a dominant role in controlling the q profile. The late-time, on-axis current distribution is, however, dominated by the NBCD, which could be improved by changes in the neutral-beam injection geometry, for example, by using off-axis NBI or with more balanced beam injection that gives lower overall NBCD. These capabilities are not presently available on DIII-D. Alternatively, control over q_0 could also be achieved by shifting the plasma to move the NBCD off axis or by using additional current drive on axis, e.g. fast-wave current drive or ECCD, to counter the NBCD. At the EC power levels soon to be available on DIII-D, significant effects should be observable during experiments. With upgrades to the ECH system, nearly full non-inductively driven configurations should be obtained on the time scales of the magnetic field pulse available on DIII-D. Density control, particularly the ability to contour the density gradient location, could provide distinct advantages for optimizing the discharge and achieving steady-state configurations. Future calculations will be directed at optimizing the combination of neutral-beam and electron-cyclotron heating and current drive to reduce the power demands and better contour the q profile for stability. By adjusting the start-up conditions and the mix of heating sources, we should be able to reduce the time require to reach steady state by minimizing the neutral beam overdrive that forces J_{OH} negative while still maintaining the NBI for heating. Recent experiments on DIII-D utilizing ECH/ECCD in quiescent double barrier (QDB) discharges [25,26] have demonstrated this strong modification of the q profile and the possibility for impurity and density profile control in a regime with density and temperature profiles similar to these NCS conditions.

REFERENCES

[1] Strait E., *et al*., Phys. Rev. Lett. **75** (1995) 4421.
[2] Rice, B.W. *et al*., Nuclear Fusion, **36** (1996) 1271.
[3] Levinton, F., *et al*., Phys. Rev. Lett. **75** (1995) 4417.
[4] Sips, A.C.C., *et al*., Plasma Phys. Control. Fusion **40** (1998) 1171.
[5] Fujita, T. *et al*., Phys. Rev. Lett. 78 (1997) 2377.
[6] Lohr, J., *et al*., Proc. of the 4th Int. Workshop on Strong Microwaves in Plasmas, Nizhny Novgorod, Russia, 1999, Vol.1, p46 (Russian Academy of Sciences, Nizhny Novgorod, 2000)
[7] Crotinger, J.A., *et al*., LLNL Report, UCRL-ID-126284, March 19, 1997.
[8] Casper, T.A. *et al.*, Proc. 23rd EPS Conference, **a096**, p295 June, 1996, Kiev, Ukraine
[9] Pearlstein, L.D. *et al.*, Proc. 28th EPS Conference on Controlled Fusion and Plasma Physics, Madeira, Portugal, June 18-22, 2001.
[10] LoDestro, L.L. and Pearlstein, L.D., Phys. Plasmas **1** (1994) 90.
[11] Goldston, R.J., *et al*., J. Comp. Physics **43** (1981) 61.
[12] Houlberg, W.A., *et al*., Phys.Plasmas **4**, (1997) 3230.
[13] Cohen, R.H., *et al*., Phys. Fluids **30** (1987) 2442.
[14] Smith, G.R., *et al*., In Proc. of the 9th Joint Workshop on ECE and ECRH, Borrego Springs, CA. 19995 (World Scientific, Singapore, 1995), p.651
[15] Lin-Liu, Y.R., *et al.*, Radio Frequency Power in Plasmas: 12th Topical Conference, CP403 (195) 1997.
[16] Casper, T. A., *et al*., Proc. 25th EPS Conference On Controlled Fusion and Plasma Physics, Prague, Czech Republic, p3.190 (p652) June 29-July 3,1998.
[17] Waltz, R.E., *et al*., Phys. Plasmas **4** 2482 (1997).
[18] Stallard, B.W., *et al*., Physics of Plasmas **6** (1999) 1978.
[19] Rogister, A.L., *et al*., Nuclear Fusion, **41** (2001) 1101.
[20] Garbet, X., *et al*., Phys. Plasmas, **6** (2001) 2793.
[21] Kinsey, J.E., *et al*., Phys. Ref. Lett. **86** (2001) 814.
[22] Lau, L., http://lithos.gat.com/efit.
[23] Glasser, A.H., LANL Report, LA-UR-95-528, February 1995.
[24] C.C. Petty, *et al*., Proc. 28th EPS Conference on Controlled Fusion and Plasma Physics, Madeira, Portugal, June 18-22, 2001.
[25] Casper, T. A., *et al*, Proc. 29th EPS Conference on Controlled Fusion and Plasma Physics, Montreux, Switzerland, June 17-21, 2002.
[26] Doyle, E.J., et al., 19th IAEA Fusion Energy Conference, EX/C3-2, Lyon, France, October 14-19, 2002.
[27] Rognlien, T.D., *et al*., Contr. Plasma Phys. **34(2/3)** 362–367 (1994).
[28] Chan, V.S., *et al*., Nuclear Fusion **22** (1982) 787.
[29] Lin-Liu, Y.R., *et al*., Proc. 26th EPS Conference on Controlled Fusion and Plasma Physics, Maastricht, The Netherlands, June 14-18, 1999.
[30] Dumont, R., et al., Phys. Plasmas 7 (2000) 4972.
[31] Murakami, M., *et al.*, Bull. Am. Phys. Soc. 46, 101 (2001) to be published in Physics of Plasmas.

ACKNOWLEDGEMENTS

The authors would like to thank Tim Luce, Pete Politzer and Tony Taylor at GA for suggesting the transport model. We would also like to acknowledge Tom Dodge (UC Davis and now at Columbia U.) for developing the feedback control algorithm during a summer project at LLNL. We also thank the DIII-D group for access to the experimental data.

FIGURE CAPTIONS

Fig. 1 DIII-D shot #92668 parameters used to initialize the ECH simulations at 1.45s.

Fig. 2 Corsica profiles at 1.46 just prior to application of EC power in simulations: (a) comparison of computed q profile with experimental fit, (b) comparison of fits to measured temperature profiles (Experiment) and profiles resulting from transport model (Corsica) at 1.46s and at an energy confinement time, τ_E*, later without ECH, (c) model thermal conductivities.*

Fig.3 Simulated flux-averaged total current density and q profiles at start of simulated EC power injection (1.5s), ~$2\tau_E$ *after 4.5MW ECH is applied (1.6s), prior to barrier loss (4.0s) and late time (7.0s) after barrier is lost.*

Fig. 4 Components of the current density profiles at t=4s, just prior to losing the barrier where J_T*=total,* J_{SB}*=bootstrap,* J_{NB}*=neutral beam and* J_{EC}*=electron cyclotron driven currents and* J_{OH} *is the Ohmic current density.*

Fig. 5 q_{min} *and* ρ_{qmin} *evolution as a function of ECH absorbed power indicating power dependence for sustaining NCS. The break in the curves occurs when the Ohmic current profile evolution dominates the ECCD and the barrier begins to move inward.*

Fig. 6 Performance curves (τ_{dur} *vs.* P_{EC}*) for ECCD to maintain* ρ_{qmin} *in NCS discharge conditions for shot 92668.* τ_{dur}*, defined as the time from onset of EC (1.5s) to the break in the* ρ_{qmin} *curve in Fig. 5, is the time duration that ECCD can hold the position of* q_{min}*.*

Fig. 7 Evolution of δW_T *(total energy = plasma + vacuum) for 4.5MW heating case using DCON for ideal stability analysis for toroidal mode numbers n=1,2 and 3.* $\delta W_T < 0$ *for instability*

Fig. 8 Equilibrium surfaces and ray trajectories from Toray-GA with aiming for ECCD at ρ*=0.425 as projected onto the (a) poloidal and (b) toroidal planes. Ray trajectories terminate when remaining power is reduced to* 10^{-4}*, e.g. total power absorption. Resonant surfaces are shown as dotted line curves in both projections.*

Fig. 9 ECCD profiles (a) and the resulting q profiles (b) with and without feedback on the antenna aiming angle during initial evolution of current distribution from 1.5s to 4s in simulations with P_{EC} *indicated. The vertical line is the desired location of peak current drive that is maintained with feedback.*

Fig. 10 ρ_{qmin} *evolution for varying* P_{EC} *using Toray-GA ray tracing code and antenna feedback controlled to hold the ECCD at* ρ*=0.425. The 12MW case is maintained to 25s (steady state).*

Fig. 11 q and current density profile components for P_{EC}=12MW at t=20s, near steady state. At steady state, $J_{OH}=0$ over entire profile and $J_T(0)=J_{NB}(0)$ resulting in a slightly higher value of q_0.

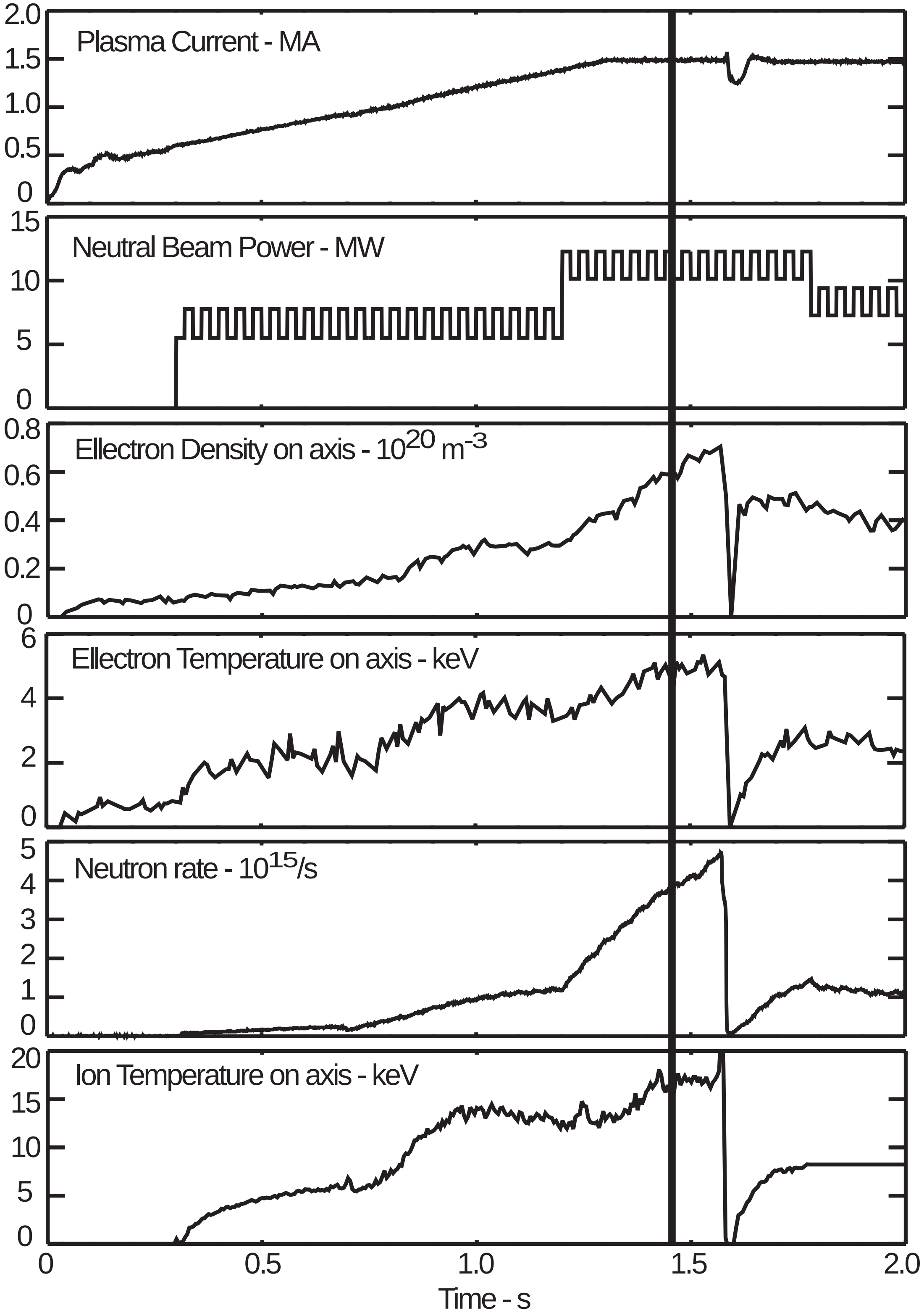
Plasma Current - MA
2.0
1.5
1.0
0.5
0
Neutral Beam Power - MW
15
10
5
0
Ellectron Density on axis - 10^{20} m^{-3}
0.8
0.6
0.4
0.2
0
Ellectron Temperature on axis - keV
6
4
2
0
Neutron rate - 10^{15}/s
5
4
3
2
1
0
Ion Temperature on axis - keV
20
15
10
5
0
0
0.5
1.0
1.5
2.0
Time - s

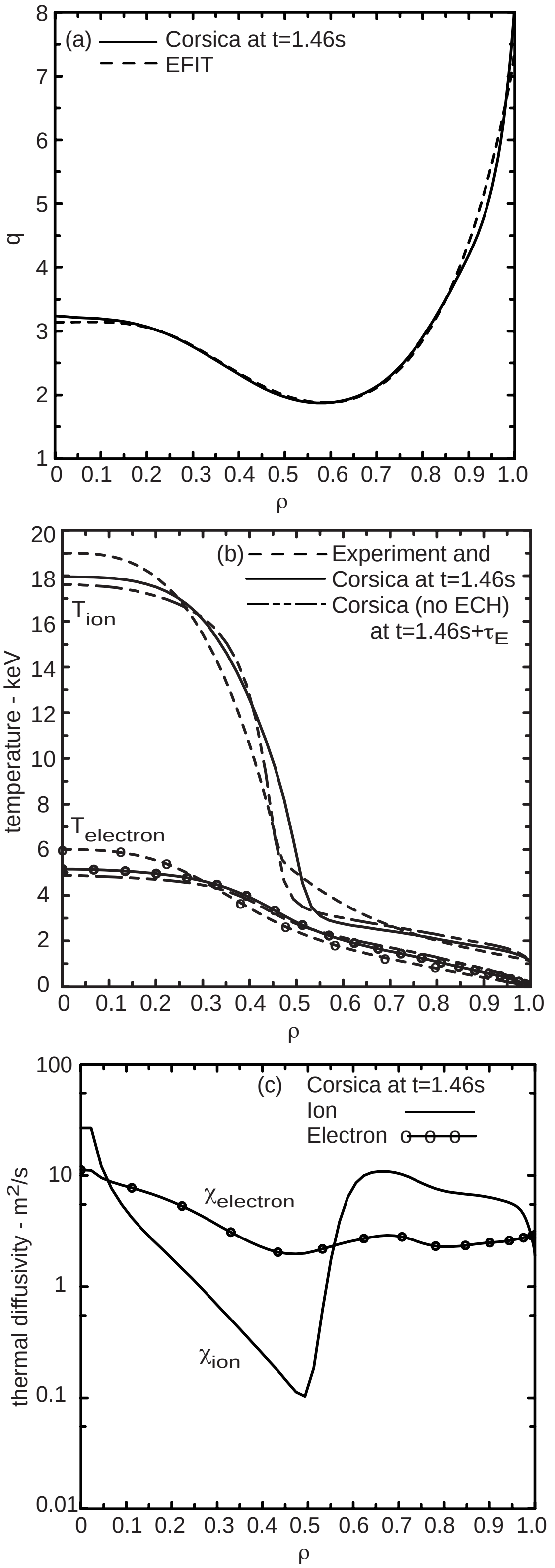
(a)
Corsica at t=1.46s
EFIT
q
1
2
3
4
5
6
7
8
0
0.1
0.2
0.3
0.4
0.5
0.6
0.7
0.8
0.9
1.0
ρ
(b)
Experiment and
Corsica at t=1.46s
Corsica (no ECH)
at t=1.46s+τ_E
T_{ion}
$T_{electron}$
temperature - keV
0
2
4
6
8
10
12
14
16
18
20
0
0.1
0.2
0.3
0.4
0.5
0.6
0.7
0.8
0.9
1.0
ρ
(c)
Corsica at t=1.46s
Ion
Electron
$\chi_{electron}$
χ_{ion}
thermal diffusivity - m^2/s
0.01
0.1
1
10
100
0
0.1
0.2
0.3
0.4
0.5
0.6
0.7
0.8
0.9
1.0
ρ

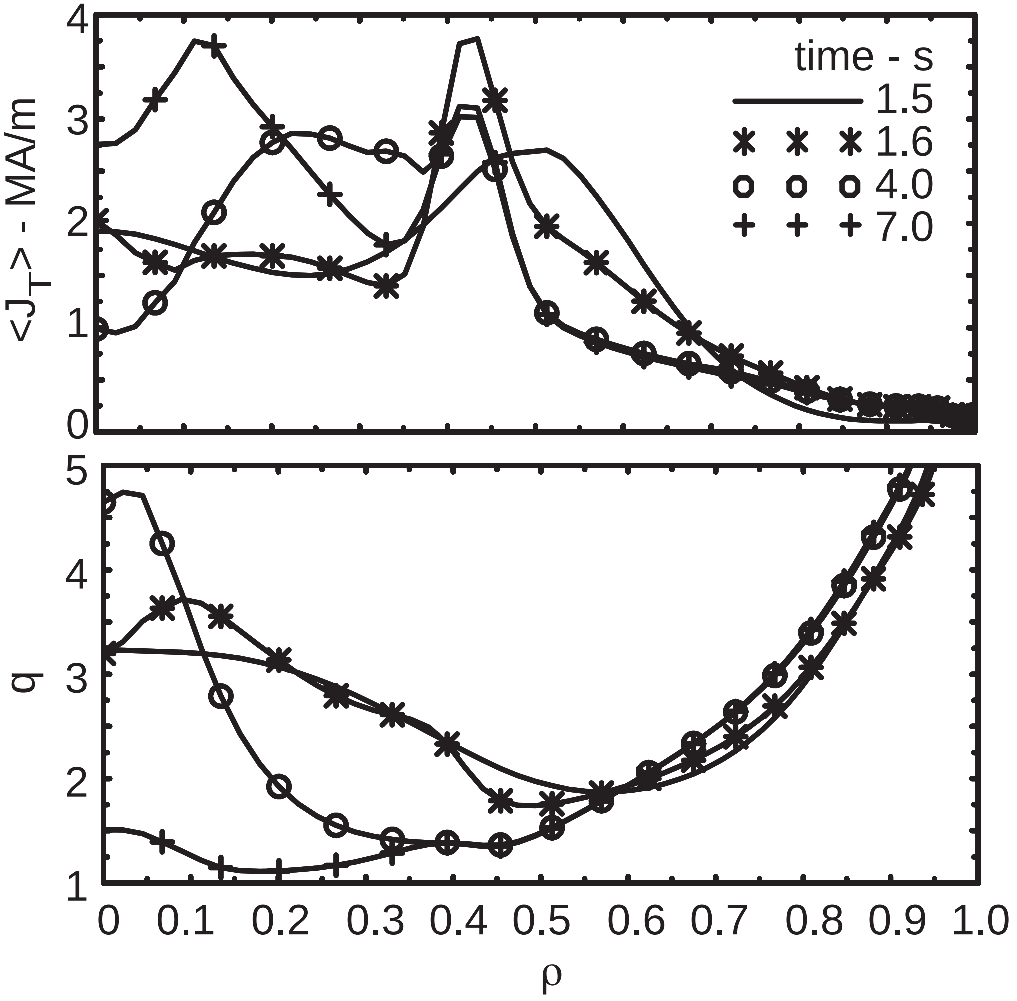

time - s
1.5
1.6
4.0
7.0
$<J_T>$ - MA/m
q
ρ
0
1
2
3
4
5
0.1
0.2
0.3
0.4
0.5
0.6
0.7
0.8
0.9
1.0

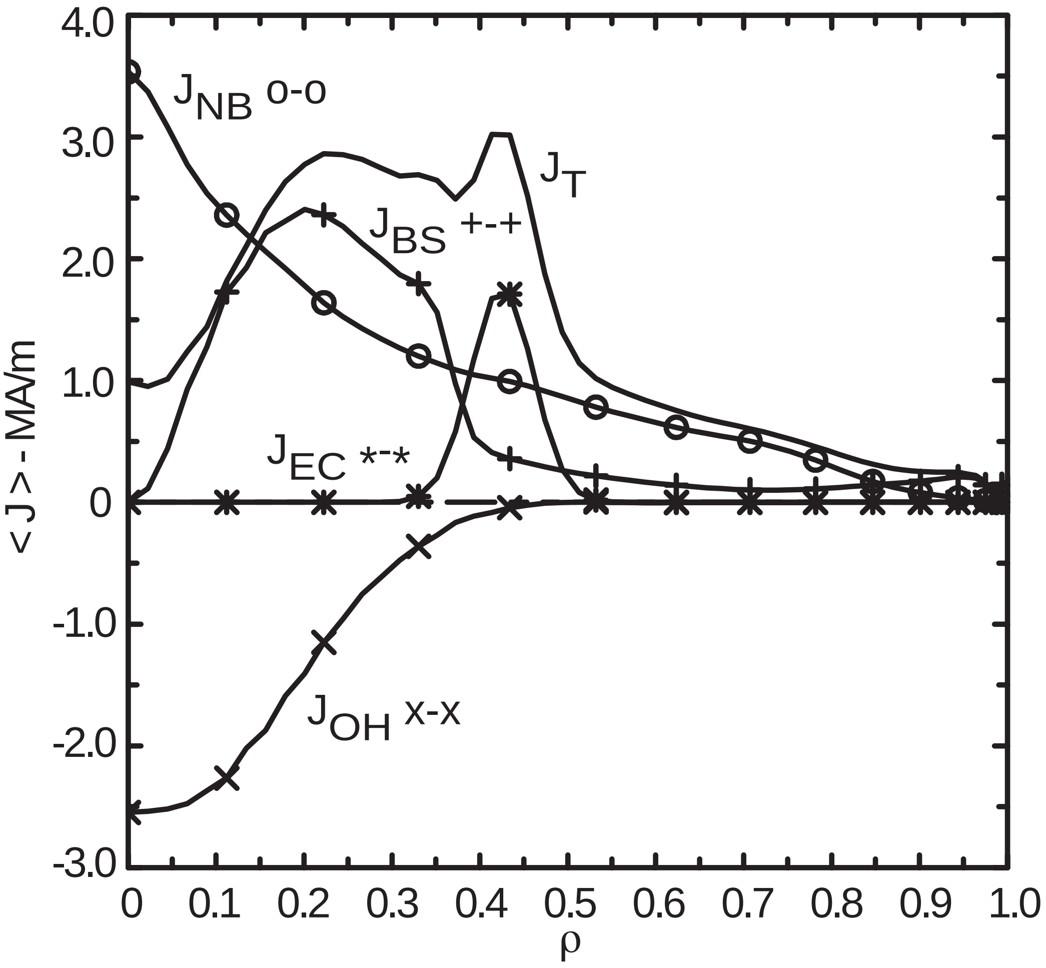

4.0
3.0
2.0
1.0
0
-1.0
-2.0
-3.0
< J > - MA/m
0
0.1
0.2
0.3
0.4
0.5
0.6
0.7
0.8
0.9
1.0
ρ
J_NB o-o
J_T
J_BS +-+
J_EC *-*
J_OH x-x

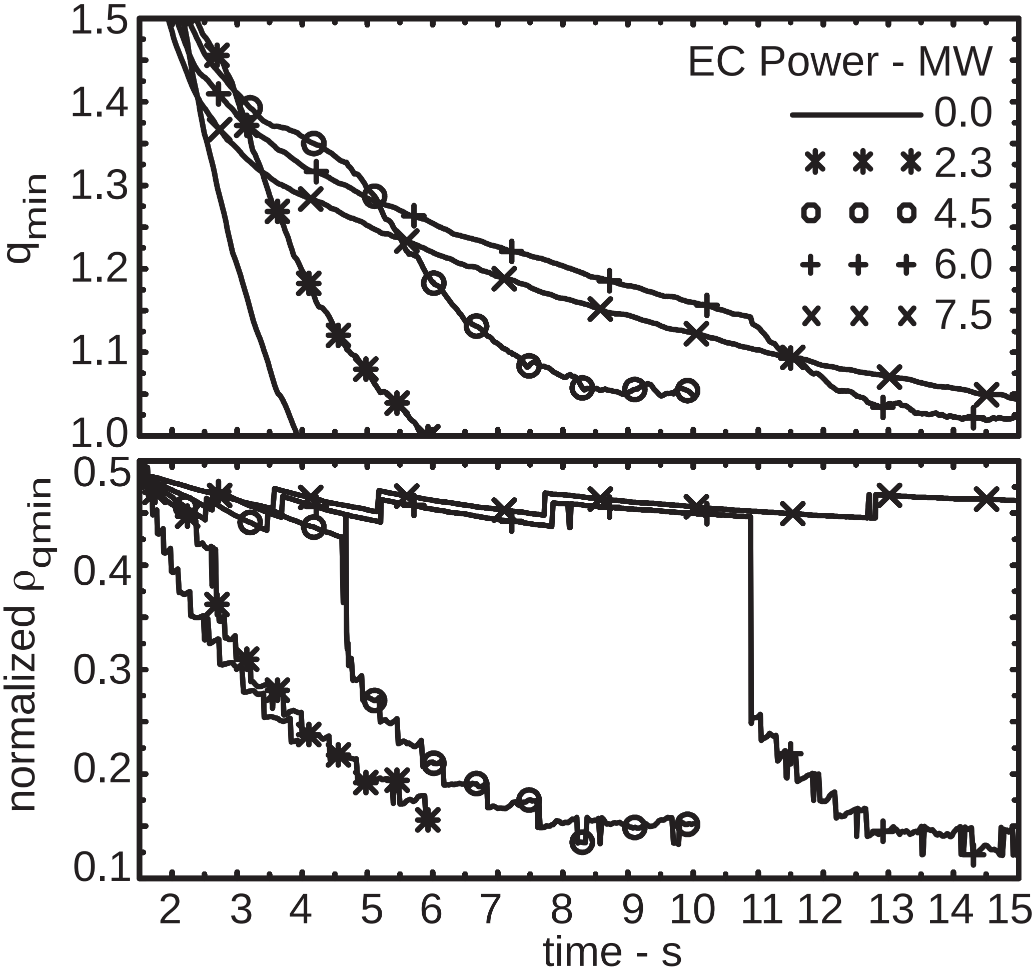
EC Power - MW
0.0
2.3
4.5
6.0
7.5
q_{min}
1.5
1.4
1.3
1.2
1.1
1.0
normalized ρ_{qmin}
0.5
0.4
0.3
0.2
0.1
2
3
4
5
6
7
8
9
10
11
12
13
14
15
time - s

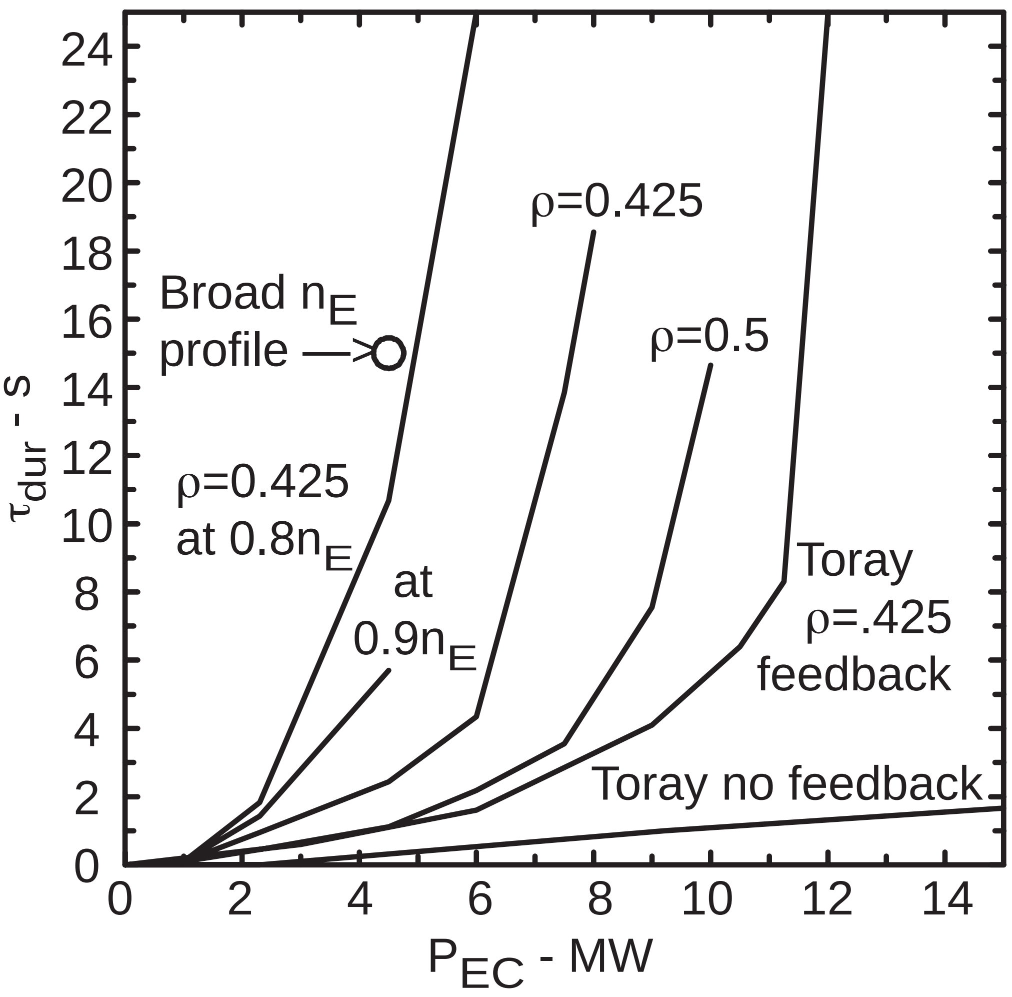
τ_{dur} - s
P_{EC} - MW
0
2
4
6
8
10
12
14
16
18
20
22
24
0
2
4
6
8
10
12
14
Broad n_E profile —>
ρ=0.425 at 0.8n_E
at 0.9n_E
ρ=0.425
ρ=0.5
Toray ρ=.425 feedback
Toray no feedback

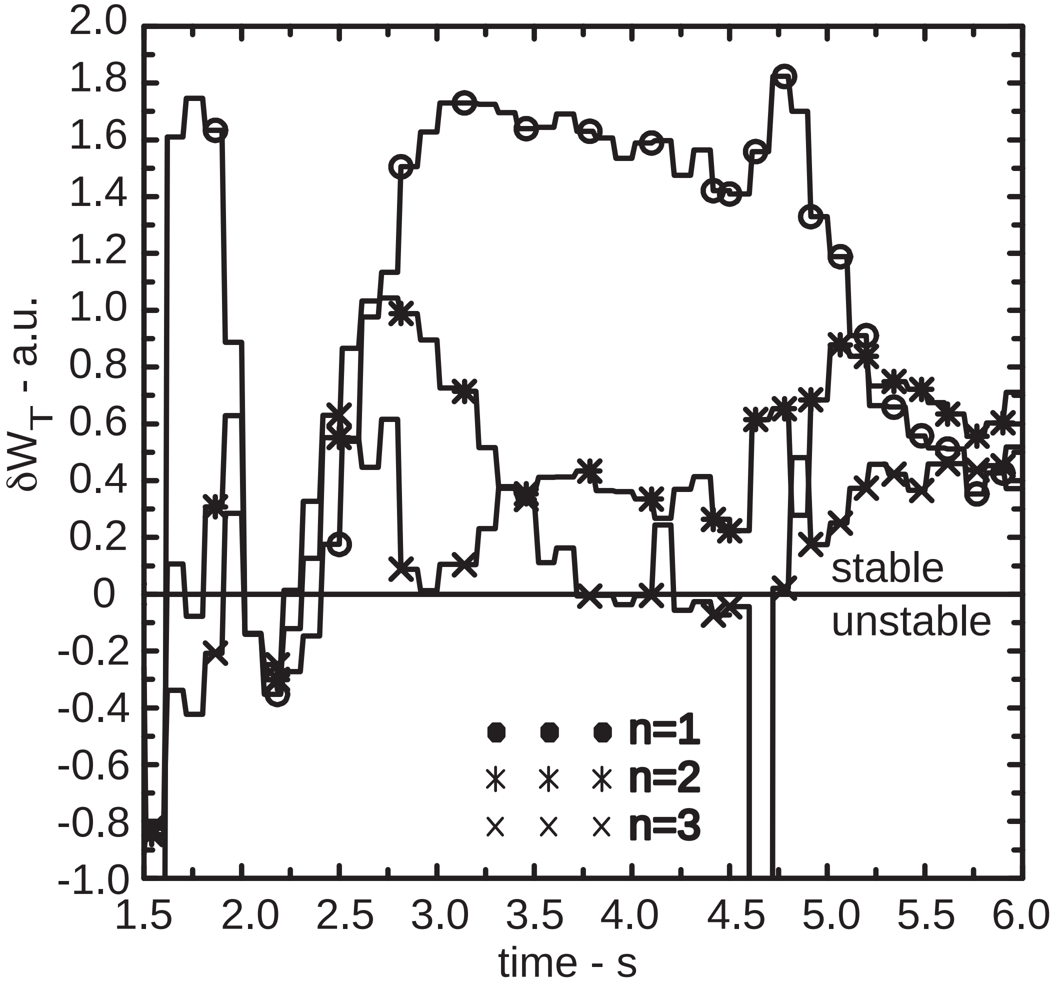
δW_T - a.u.
2.0
1.8
1.6
1.4
1.2
1.0
0.8
0.6
0.4
0.2
0
-0.2
-0.4
-0.6
-0.8
-1.0
1.5
2.0
2.5
3.0
3.5
4.0
4.5
5.0
5.5
6.0
time - s
stable
unstable
● ● ● n=1
⁎ ⁎ ⁎ n=2
× × × n=3

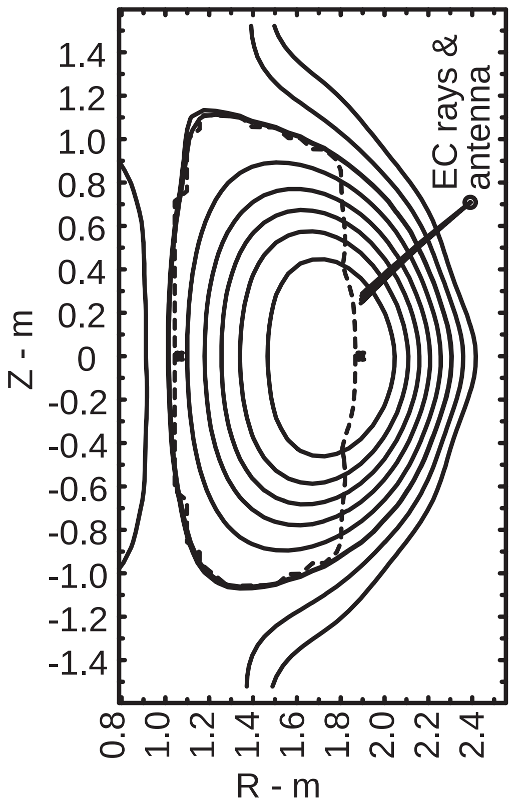

(a) Poloidal plane projection

$2\omega_{ce}$ resonance - - - - -

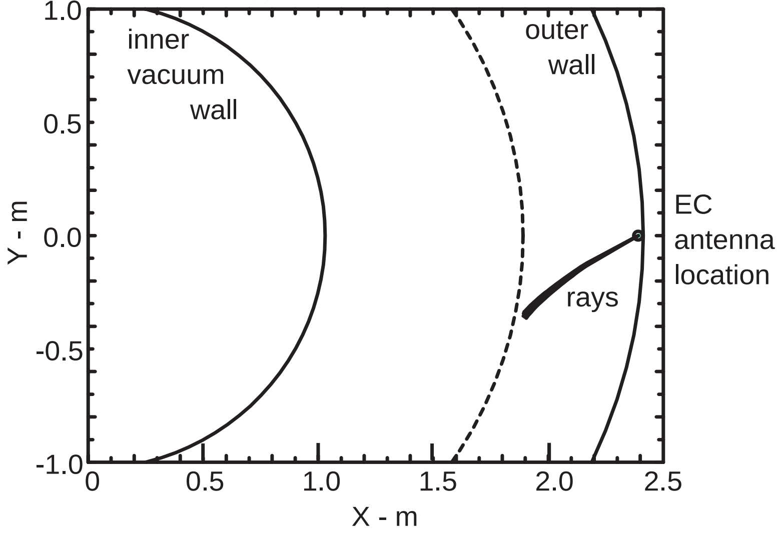

(b) Toroidal (axis) plane projection

$2\omega_{ce}$ resonance - - - - -

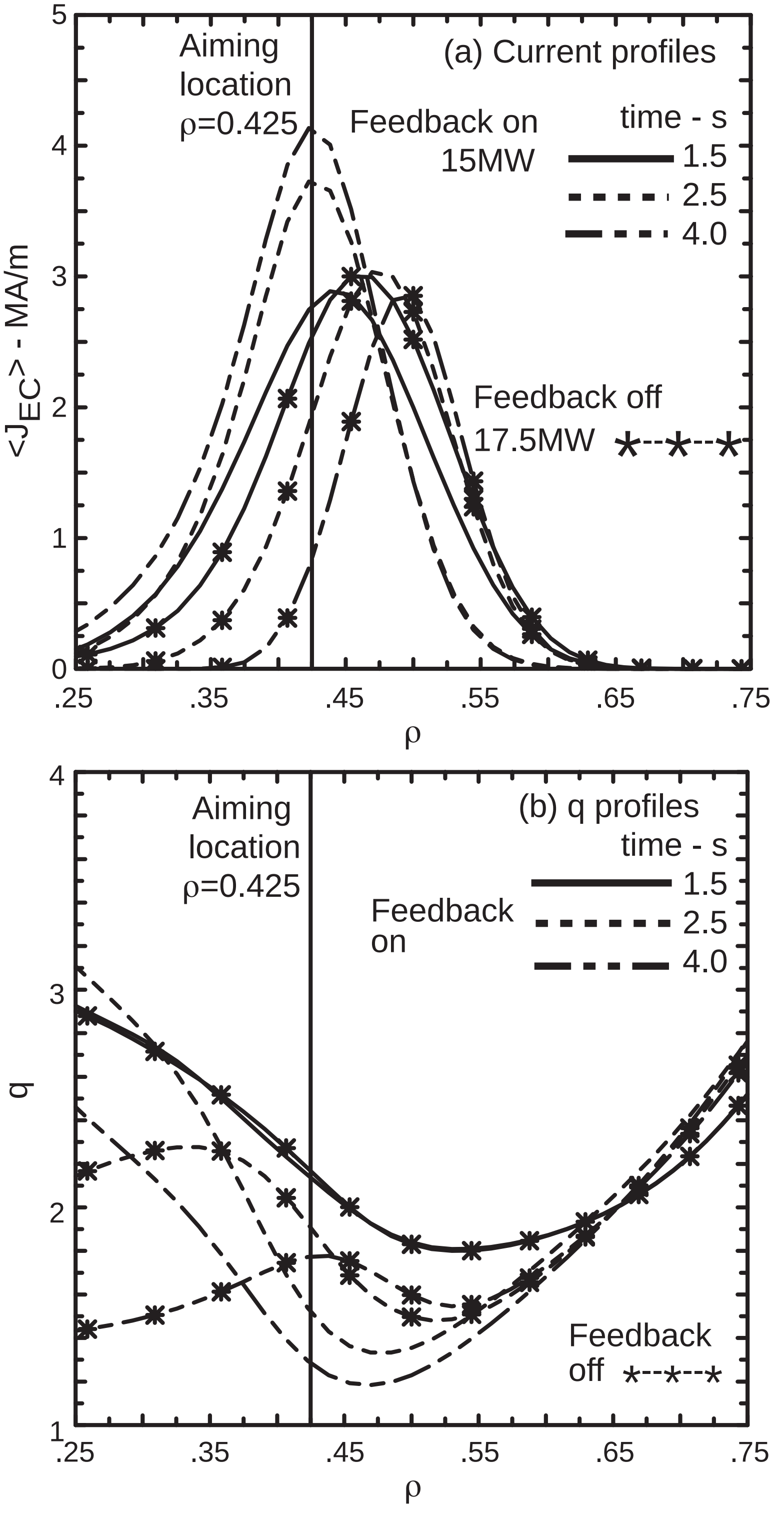

(a) Current profiles
Aiming location ρ=0.425
Feedback on 15MW
time - s
1.5
2.5
4.0
Feedback off 17.5MW
<J_{EC}> - MA/m
0
1
2
3
4
5
.25
.35
.45
.55
.65
.75
ρ
(b) q profiles
Aiming location ρ=0.425
time - s
Feedback on
1.5
2.5
4.0
Feedback off
q
1
2
3
4
.25
.35
.45
.55
.65
.75
ρ

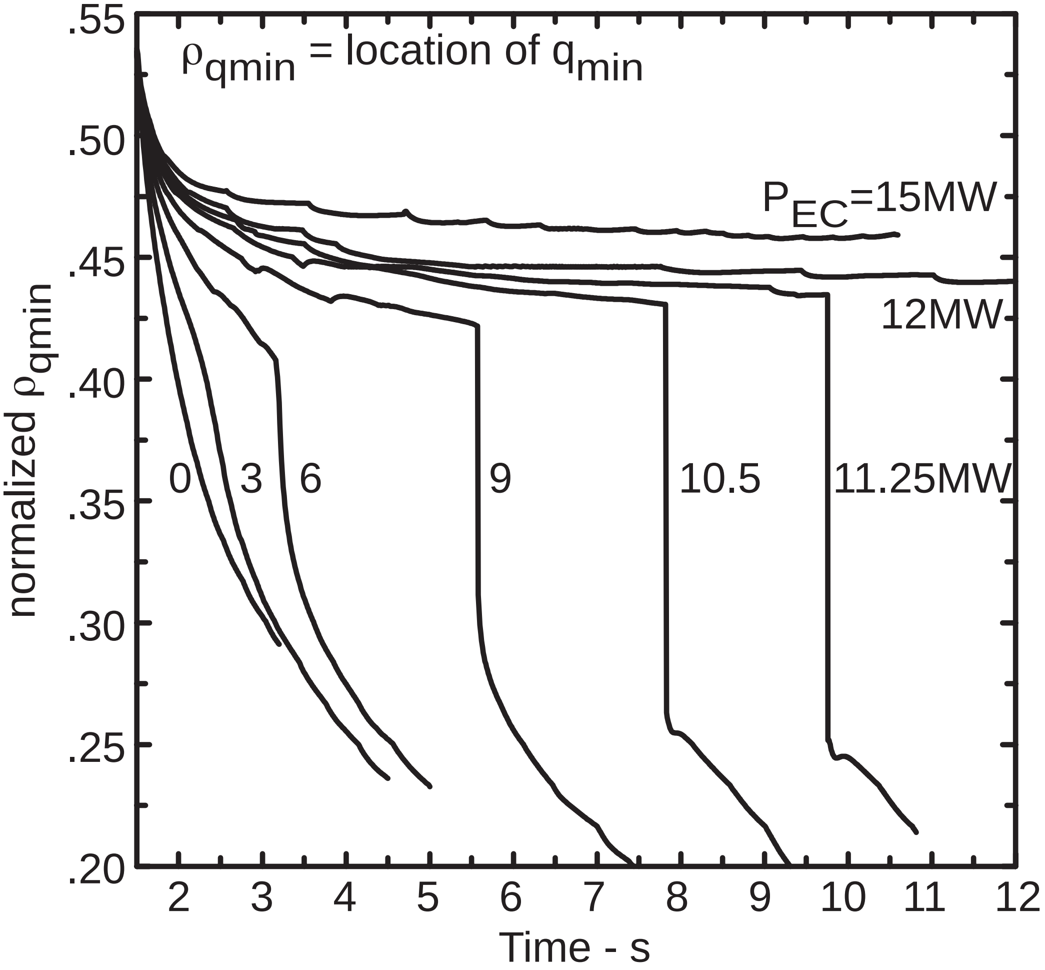

ρ_{qmin} = location of q_{min}
P_{EC}=15MW
12MW
0
3
6
9
10.5
11.25MW
normalized ρ_{qmin}
.55
.50
.45
.40
.35
.30
.25
.20
2
3
4
5
6
7
8
9
10
11
12
Time - s

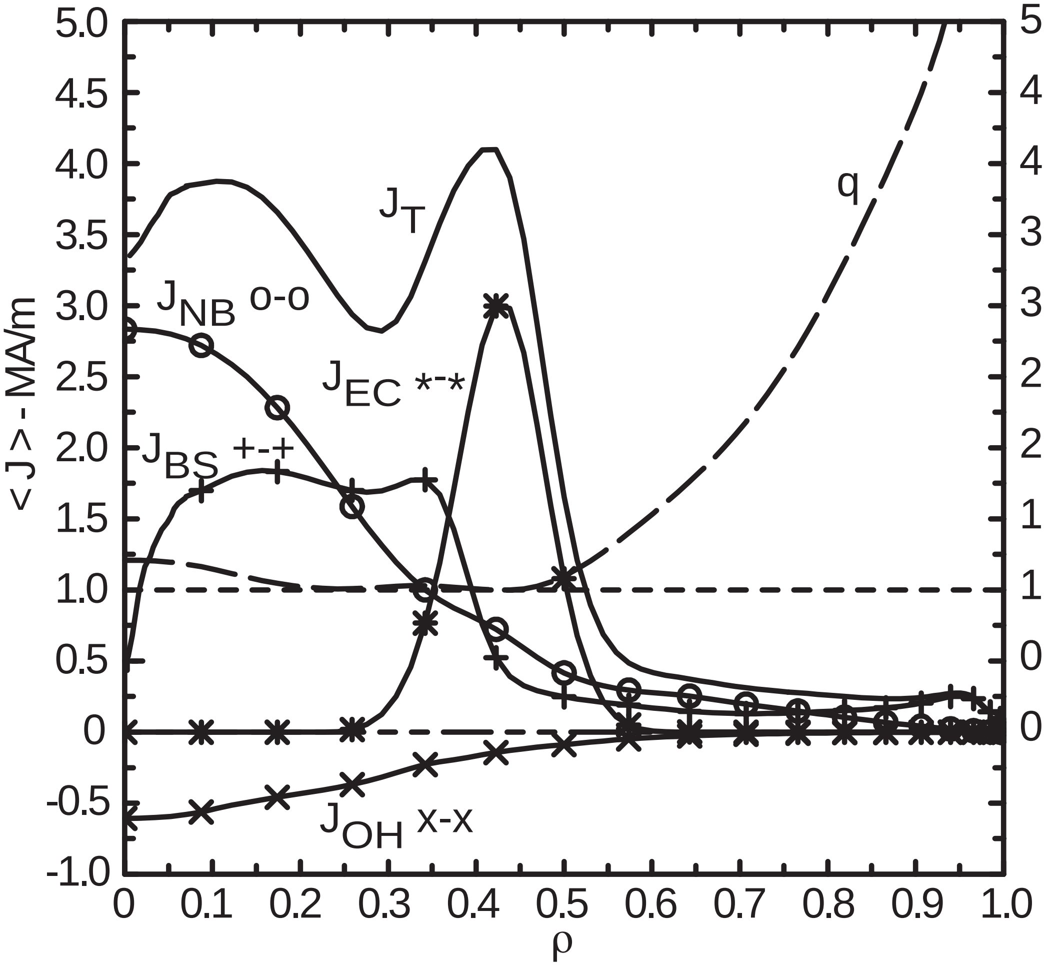
5.0
4.5
4.0
3.5
3.0
2.5
2.0
1.5
1.0
0.5
0
-0.5
-1.0
< J > - MA/m
q
J_T
J_NB o-o
J_EC *-*
J_BS +-+
J_OH x-x
0
0.1
0.2
0.3
0.4
0.5
0.6
0.7
0.8
0.9
1.0
ρ

University of California
Lawrence Livermore National Laboratory
Technical Information Department
Livermore, CA 94551